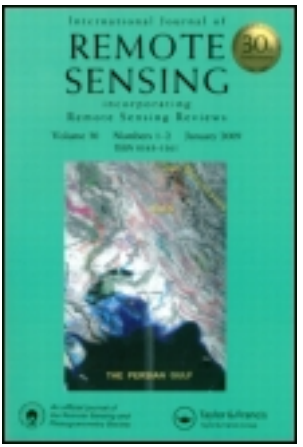

International Journal of Remote Sensing

Publication details, including instructions for authors and subscription information:
http://www.tandfonline.com/loi/tres20

Numerical modelling of transspectral processes in natural waters: Implications for remote sensing

H. Grassl, D. Pozdnyakov, A. Lyaskovsky & L. Pettersson

Available online: 25 Nov 2010

To cite this article: H. Grassl, D. Pozdnyakov, A. Lyaskovsky & L. Pettersson (2002): Numerical modelling of transspectral processes in natural waters: Implications for remote sensing, International Journal of Remote Sensing, 23:8, 1581-1607

To link to this article: http://dx.doi.org/10.1080/014311601170735

INT. J. REMOTE SENSING, 2002, VOL. 23, NO. 8, 1581–1607

Numerical modelling of transspectral processes in natural waters: implications for remote sensing

D. POZDNYAKOV, A. LYASKOVSKY

Nansen International Environmental and Remote Sensing Centre, 18 Korpousnaya str., 197110, St. Petersburg, Russia; e-mail: dmitry.pozdnyakov@niersc.spb.ru; anton@niersc.spb.ru

H. GRASSL

Max-Planck-Institute for Meteorology, Bundesstrasse 55, D-20146 Hamburg, Germany; e-mail: grassl@dkrz.de

and L. PETTERSSON

Nansen Environmental and Remote Sensing Centre, Edv.Griegsv. 3A N-5037 Solheimsviken Norway; e-mail: lasse.pettersson@nrsc.no

(*Received 7 February 2000; in final form 24 May 2001*)

Abstract. Based on a previously developed and thoroughly validated hydro-optical model, numerical simulations of the spectral composition of water leaving radiance are presented. These simulations take into account absorption, elastic scattering, water Raman (inelastic) scattering as well as the fluorescence of chlorophyll (*chl*) and dissolved organics (*doc*). The results obtained for forward modelling were also used for the inverse problem: retrieval of water quality parameters from water volume reflectance (R) spectra. The Levenberg-Marquardt multivariate optimization procedure was used for this purpose. Unlike water Raman scattering, the *chl* and *doc* fluorescence has an impact on R, so the retrieval results can change substantially for waters rich in *chl* or *doc*. Suspended minerals (*sm*) suppress both the *chl* and *doc* fluorescence influence on R. The retrieval results indicate that *chl* can be accurately assessed if the concentration of *sm* is not low and the *doc* concentration is $\leqslant 2\,\mathrm{mgC\,l^{-1}}$. For waters devoid of *doc*, the concentration of *chl* can be accurately retrieved even if the *sm* concentration is very low. Retrieval errors prove to be strongly dependent on the fluorescence yield value of both *chl* and *doc*.

1. Introduction

Until recently, most hydro-optical models that had been suggested as a basis for the retrieval of water quality parameters from water colour data considered only the effects of elastic scattering and absorption on the water leaving radiance (see e.g. Bukata *et al.* 1995). At the same time, enough evidence had been compiled that together with water Raman inelastic scattering, fluorescence by both chlorophyllous pigments in phytoplankton and dissolved organics can appreciably affect the spectral distribution of upwelling radiance, and hence water colour (see e.g. Sugihara *et al.* 1984, Fischer and Kronfeld 1990, Vodacek *et al.* 1994, Waters 1995, Coble and

International Journal of Remote Sensing
ISSN 0143-1161 print/ISSN 1366-5901 online © 2002 Taylor & Francis Ltd
http://www.tandf.co.uk/journals
DOI: 10.1080/01431160110070735

Brophy 1996). This evidence has warranted the development of models simulating the above processes (Gordon 1979, Marshall and Smith 1990, Haltrin and Kattawar 1993, Sathyendranath and Platt 1998, Vodacek *et al.* 1994), which are often called transspectral since stimulation at wavelength λ_1 leads to emissions at λ_2 with $\lambda_2 > \lambda_1$.

In this paper we use numerical experiments to analyse the importance of water Raman scattering and fluorescence by chlorophyll and dissolved organics, for precise retrieval of water quality parameters. To achieve this goal, first we investigate the sensitivity of water leaving radiance to individual and concerted impacts of the above transspectral processes, and to variations in concentrations of the major optically-active water constituents, namely phytoplankton chlorophyll, suspended minerals and dissolved organics. Secondly, we analyse the influence of inelastic scattering and fluorescence on radiometric characteristics of water colour, such as the dominant wavelength and colour purity. Finally, we compare the simulation results with our previous studies (Bukata *et al.* 1997), which did not consider these solar light interactions in natural waters, and discuss the implications for water colour observations of the world's oceans and fresh water bodies.

2. Methodology

2.1. *Forward problem solution*

Of all the radiance components captured by a remote sensor when viewing a water body, only the radiance $L_u(+0, \lambda)$ coming up from beneath the water surface provides information on both the water quality and the nature of sunlight photon interactions in the aquatic medium. The forward problem in the context of remote sensing thus consists of reproducing $L_u(+0, \lambda)$.

However, being a function of both water optical properties and incident radiation, $L_u(+0.\ \lambda)$ *per se* is inconvenient for analysing the impact of in-water light transfer processes on the signal sought. Rather, the water volume reflectance R, to which $L_u(+0.\ \lambda)$ is unambiguously related, is a better candidate for this purpose. Indeed, the optical behaviour of natural waters is a consequence of quantities that are *inherent* to the water body itself, namely (a) coefficients of light absorption, (b) scattering and (c) attenuation. These *inherent optical properties* (IOP) determine the aquatic medium impact on the subsurface radiation field that manifests itself through *apparent optical properties* (AOP) amongst which is the volume reflectance R.

By definition, $R(\lambda, z)$ is defined as the upwelling radiance $E_u(\lambda, z)$ at a depth z beneath the air–water interface normalized to the downwelling irradiance $E_d(\lambda, z)$ at the same depth. In a single scattering approximation, the upwelling light fields originating from sources of different nature can be treated as independent (Gordon 1979), and the bulk apparent optical property $R(\lambda, z)$ can consequently be considered as the additive result of the individual AOP arising from each kind of sunlight interaction within the water column, such as absorption and elastic scattering in a semi-infinite aquatic medium $R_{e.s.}$, inelastic (Raman) scattering R_r, chlorophyll fluorescence R^f_{chl}, and dissolved organics fluorescence R^f_{doc}. In reality, when also considering the transspectral processes such as Raman scattering or fluorescence, whose phase functions are nearly isotropic, multiple, downward-scattering events may need to be included. However, Sathyendranath and Platt (1998) have shown that, typically, the contribution to water Raman of photons scattered twice or three times would only be in the order of 10% of the contribution from single scattering. The contribution of even higher orders, the fourth and fifth, would again be only around 10% that of orders two and three. It is not unreasonable to assume that this should also

hold for fluorescence by chlorophyll and dissolved organics (Sathyendranath and Platt 1998).

The following sections describe which relations and simplifications we have used in our forward model, which calculates $R(\lambda, z)$.

2.1.1. *Elastic scattering*

A number of relationships are suggested for relating $R_{e.s.}$ to IOP (see e.g. Bukata *et al.* 1995). Recently, the efficiency of some of the suggested formulations has been validated against the field data obtained in Saginaw Bay of Lake Huron (Pozdnyakov *et al.* 1999). It was found that, although all expressions tested provided very similar results, corresponding well to the actual measurements (Gordon *et al.* 1975, Kirk 1981, Jerome *et al.* 1988), the equation suggested by Jerome *et al.* seems to be less vulnerable to the remarkable optical heterogeneity of Saginaw Bay at sun zenith angles not exceeding $\approx 50°$. Therefore it is believed to be more appropriate for simulations of widely varying hydrooptical situations.

$$\begin{aligned} R_{e.s.}(-0) &= (1/\mu_0)0.319 b_b/a && \text{for } 0 \leqslant b_b/a \leqslant 0.25, \text{ and} \\ R_{e.s.}(-0) &= (1/\mu_0)[\,0.013 + 0.267 b_b/a] && \text{for } 0.25 \leqslant b_b/a \leqslant 0.50, \end{aligned} \tag{1}$$

where $\mu_0 = \cos(\theta_0')$, θ_0' being the in-water refracted angle, $b_b = Bb$, B being the backscattering probability; $\mu_0 = 0.858$ for overcast conditions, (-0) indicating just beneath the water surface.

2.1.2. *Water Raman scattering*

Barlett (1997) quantitatively compared four models developed by Marshall and Smith (1990), Lee et al. (1994), Haltrin and Kattawar (1993) and Sathyendranath and Platt (1998) for describing the effect of Raman scattering on the upwelling irradiance in natural water. This comparison has shown that the model by Sathyendranath and Platt (1998) is the most easily applicable and gives adequate results. The model can be represented as:

$$\begin{aligned} R_r(\lambda_{em}, -1) = {} & \frac{b_{b_r}(\lambda_{ex}) E_d(\lambda_{ex}, -0)}{2\mu_d (K_u(\lambda_{em}) + K_d(\lambda_{ex})) E_d(\lambda_{em}, -0)} \\ & \times \left[1 + \frac{\mu_d}{\mu_u} R_\infty(\lambda_{ex}, -0) + \frac{b_b(\lambda_{em})}{2\mu_u K_u(\lambda_{em})} \right] \end{aligned} \tag{2}$$

where $b_{b_r}(\lambda)$ is the Raman coefficient for backscattering, $b_{b_r}(\lambda) = B_r b_r(\lambda)$, B_r = inelastic backscattering probability, $b_r(\lambda)$ = coefficient of Raman scattering, $b_b(\lambda)$ = elastic backscattering coefficient, $K_d(\lambda)$, $K_u(\lambda)$ = irradiance attenuation coefficients for downwelling and upwelling fluxes, respectively, μ_d, μ_u = average cosines for downwelling ($E_d(\lambda)$) and upwelling ($E_u(\lambda)$) irradiances, respectively, λ_{ex} and λ_{em} = Raman scattering excitation and emission wavelengths, respectively.

In deriving equation 2 it was assumed that the water body is vertically homogeneous, optically thick and not excessively absorption-dominated (see Barlett 1996 for details).

According to Sugihara et al. (1984), the relationship between λ_{em} (corresponding to the maximum intensity in the Raman spectrum) and λ_{ex} can be approximated as

$$\lambda_{em,\max} = \frac{\lambda_{ex}}{-3357 \,.\, 10^{-7} \lambda_{ex} + 1} \tag{3}$$

Expressions derived by Kirk (1984) can be used to obtain the attenuation coefficients for direct incident solar radiation, $K_{sun}(\lambda, \theta'_0)$, and for diffuse incident sky radiation, $K_{sky}(\lambda)$, namely:

$$K_{sun}(\lambda, \theta'_0) = (\cos \theta'_0)^{-1} [a(\lambda)^2 + (0.473 \cos \theta'_0 - 0.218) a(\lambda) b(\lambda)]^{1/2} \quad (4)$$

and

$$K_{sky}(\lambda) = 1.168 [a(\lambda) + 0.168 a(\lambda) b(\lambda)]^{1/2} \quad (5)$$

where $a(\lambda)$ and $b(\lambda)$ are, as above, the bulk absorption and bulk scattering coefficients for the aquatic medium, and θ'_0 is the refracted solar zenith angle as measured immediately below the air-water interface.

The combined downwelling irradiance attenuation coefficient $K_d(\lambda, \theta'_0)$ is given as:

$$K_d(\lambda, \theta'_0) = F_w K_{sky}(\lambda) + (1 - F_w) K_{sun}(\lambda, \theta'_0) \quad (6)$$

where $F_w = F(1 - \rho_{sky})[F(1 - \rho_{sky}) + (1 - F)(1 - \rho_{sun}(\theta_0))]^{-1}$, ρ_{sky} = Fresnel reflectivity of sky irradiance for a flat air–water interface, $\rho_{sun}(\theta_0)$ = Fresnel reflectivity of solar irradiance propagating with the zenith angle θ_0, and $F = E_{sky}/(E_{sky} + E_{sun})$ is the diffuse fraction of the above surface downwelling global irradiance which is a sum of direct (E_{sun}) and diffuse (E_{sky}) components.

Assuming a uniform diffuse radiance distribution of the sky, it is approximately constant for all angles. For clear skies the value of ρ_{sky} averaged over the visible range is 0.066 (Burt 1953), whereas for completely overcast skies (assuming a cardioidal distribution) it is somewhat lower—0.052 (Preisendorfer 1957).

Fresnel's equation for unpolarized light gives the reflectance of a direct beam (Jerlov 1976):

$$\rho_{sun}(\lambda, \theta_0) = 1/2 \left[\frac{\sin^2(\theta_0 - \theta'_0)}{\sin^2(\theta_0 + \theta'_0)} + \frac{\tan^2(\theta_0 - \theta'_0)}{\tan^2(\theta_0 + \theta'_0)} \right] \quad (7)$$

Snell's law describes the relationship between θ_0 and θ'_0 : $\sin \theta_0 / \sin \theta'_0 = n_w / n_a$, where the ratio of the refractive index of water (n_w) to the refractive index of air (n_a) is 1.341 (Jerlov 1976).

For a calm water surface, the downwelling subsurface irradiance $E_d(\lambda, -0)$ can be directly estimated from above-surface values of downwelling irradiance $E_d(\lambda, +0, \lambda_0)$ through the following relationship (Baker and Smith 1997):

$$E_d(\lambda, -0, \theta_0) = \frac{1}{1 - \rho_u(\theta_0)} [(1 - \rho_{sun}(\theta_0)) E_{sun}(\lambda, \theta_0) + (1 - \rho_{sky}) E_{sky}(\lambda)] \quad (8)$$

where $\rho_u(\theta_0)$ is the coefficient of reflection of subsurface upwelling irradiance for solar zenith angle θ_0. According to Jerome *et al.* (1988):

$$\rho_u(\theta_0) = 0.271 + 0.249 \mu_0 \quad (9)$$

for direct incident solar radiation, and $\rho_u = 0.561$ for a cardioidal diffuse incident radiation distribution, μ_0 being, as above, the in-water refracted angle to be calculated from Snell's law. In some earlier works (Gordon 1969), as quoted by Baker and Smith (1997), ρ_u varied from 0.485 to 0.463, decreasing as wind speed increased from 0 to 16 m s^{-1}.

2.1.3. *Fluorescence of chlorophyll and dissolved organics.*

Gordon (1979) modified the radiative transfer equation to include the effect of fluorescent substances (phytoplankton chlorophyll *a* as an example) and solved it in the quasi-single scattering approximation for a vertically homogeneous ocean containing fluorescent particles with wavelength independent quantum efficiency (η_{chl}) and a Gaussian shaped emission line. For a wavelength of maximum emission (λ_{0em}), the volume reflectance R^f arising from an aquatic constituent fluorescence can be expressed at the maximum of the emission line (i.e., at $\lambda = \lambda_{0em}$) as follows:

$$R^f = \frac{\eta}{\sqrt{2\pi\sigma^2}} \exp\left(- \frac{(\lambda_{em} - \lambda_{0em})^2}{2\sigma^2} \right) / 2K_d(\lambda_{em}) \mu_0 \mathrm{E}_d(\lambda_{em}, -0) \lambda_{em} \times \int_{\lambda_{ex}} \lambda_{ex} a_f(\lambda_{ex}) E_d(\lambda_{ex}, -0) f(\lambda_{ex}, \lambda_{em}) d\lambda_{ex} \quad (10)$$

where λ_{ex} and λ_{em} are the excitation and emission wavelengths respectively, $a_f(\lambda)$ is the fluorophore absorption coefficient, is the half-width of the fluorescence band with a Gaussian shape,

$$f(\lambda_{ex}, \lambda_{em}) = \frac{K_d(\lambda_{em})}{K_d(\lambda_{ex})} \left[1 - \frac{K_d(\lambda_{em})}{K_d(\lambda_{ex})} \ln\left(1 + \frac{K_d(\lambda_{ex})}{K_d(\lambda_{em})} \right) \right] \quad (11)$$

Vodacek *et al.* (1994) suggested an experimental model of the solar-stimulated fluorescence of chromophoric dissolved organic matter. This model was extended by Green and Blough (1994) in terms of establishing characteristic values and spectral variations of the *doc* fluorescence quantum yield, $\eta_{doc}(\lambda)$, and the absorption coefficient, $a_{doc}(\lambda)$. The model provided a conversion of the relative fluorescence to absolute photon numbers (through normalizing η to that of quinine sulfate), and unlike the above model, used an experimentally determined shape factor, otherwise being analogous to the formulism of Gordon (1979).

Later, considering the fluorescence emitted from a small volume of a water column, Culver and Perry (1997) suggested the following model for the fluorescence-driven upwelling irradiance E_u^f at a depth z in a vertically homogeneous water column:

$$E_u^f(\lambda_{em}, z) = \tfrac{1}{2} \Psi(\lambda) \int_{\lambda_1}^{\lambda_2} \frac{E_{d0}(\lambda_{ex}, z)}{K_d(\lambda_{ex}) + K_u^f(\lambda_{em})} d\lambda_{ex} \quad (12)$$

where, $\Psi(\lambda) = \eta_f(\lambda_{ex}) S_f(\lambda_{em}) \int_{\lambda_1}^{\lambda_2} a_f(\lambda_{ex}) d\lambda_{ex}$, η_f = quantum yield, S_f = shape factor and a_f = absorption coefficients of the fluorophore, $E_{d_0}(\lambda)$ = downwelling scalar irradiance, K_u^f is the diffuse attenuation coefficient for the upwelling fluorescent flux.

Following Gordon (1979), Culver and Perry (1997) assume that in the case of phytoplankton the shape factor S_f can be approximated by a Gaussian distribution. Furthermore, based on considerations of the angular distribution of the subsurface light field (isotropic for fluorescence and inverse to the mean cosine for solar downwelling irradiance), Culver and Perry suggest that, near the surface (i.e. $z = -0$) the following relationships hold: $K_u^f(\lambda_{em}) = \mu_0 K_d(\lambda_{em})$ and $E_d^{\,0}(\lambda) = E_d(\lambda)(\mu_0)^{-1}$. With these assumptions in mind, the volume reflectance component originating from

an aquatic constituent fluorescence can be expressed as:

$$R^f(\lambda_{em}) = \frac{1}{2\sqrt{2\pi\sigma^2}} \exp\left(-\frac{(\lambda_{em}-\lambda_{0em})^2}{2\sigma^2}\right) \times \int_{\lambda_{ex}} \eta_d(\lambda_{ex}) a_f(\lambda_{ex}) \frac{1}{\mu_0(K_d(\lambda_{ex})+2\mu_0 K_d(\lambda_{em}))} d\lambda_{ex} \quad (13)$$

By comparing equations 10 and 11, it is seen that both expressions would become very similar if the limitations of Gordon's model (wavelength independence of η, and assessment of R at the maximum of the emission line) are lifted. However, in our numerical experiments we tried both models to assess how far the simulation results differ from each other for the same hydro-optical situation and water surface illumination conditions.

2.1.4. *Radiometric water colour characterization.*

The human eye senses water colour by capturing and analysing the radiance upwelling from the water surface. This signal consists of two components $L_{w,s}(+0, \lambda)$ and $L_u(+0, \lambda)$ originating from the light reflected from the water surface, and back-scattered by the water column into the atmosphere, respectively. Only the second component carries the information about the colorimetric properties of the water column.

The relationship between the radiance coming up from beneath the water surface $L_u(+0, \lambda)$ and the water volume reflectance $R(\lambda)$ (and therefore the IOP, see above) can be given as (Austin 1974):

$$L_u(+0, \lambda) = R(\lambda)[1-\rho(\theta_v)] E_d(+0, \lambda)(1-\rho_{irr})/Qn^2[1-0.48R(\lambda)] \quad (14)$$

where $\rho(\theta_v)$ = internal reflectivity for the in-water refracted angle θ_v corresponding to the remote sensing instrument viewing angle, n, as above, is the relative index of refraction of water to air, ρ_{irr} is the surface reflectivity for downwelling irradiance in air, $E_d(+0, \lambda)$ is the incident irradiance, Q is the ratio of the upwelling irradiance just beneath the air–water interface to the upwelling nadir radiance beneath the air–water interface.

The upwelling radiance spectra are related to visual colour through chromaticity analyses, which integrate the sensitivity of the human eye with an impinging energy spectrum. Such an integration produces tristimulus values X', Y' and Z' given by (Anonymous 1957):

$$\begin{aligned} X' &= \int x''(\lambda) L_u(+0, \lambda)\, d\lambda \\ Y' &= \int y''(\lambda) L_u(+0, \lambda)\, d\lambda \\ Z' &= \int z''(\lambda) L_u(+0, \lambda)\, d\lambda \end{aligned} \quad (15)$$

where x'', y'', z'' are the CIE (Comite' International d'Eclairage) colour mixtures (for red, green and blue respectively) for equal energy spectra and may be obtained from CIE tables (Anonymous 1957).

The chromaticity coordinates could then be obtained from the equations:

$$\begin{aligned} x &= X'/(X'+Y'+Z') \\ y &= Y'/(X'+Y'+Z') \\ z &= Z'/(X'+Y'+Z') \end{aligned} \quad (16)$$

So far as $x+y+z=1$, two chromaticity coordinates adequately represent colour in a chromaticity diagram, and the chromaticities can be displayed as 2D plots of either y (green)–z (blue) or x (red)–y (green).

CIE chromaticity coordinates may be obtained for each wavelength throughout the visible spectrum. When plotted, all the (x, y) or (y, z) pairs obtained in such a manner delineate the so-called curve envelope or 'colour triangle'. For a white light, $x=y=z=0.333$. This defines the achromatic colour or white point. A numerical value of colour is then obtained by drawing a line from this white point through the plotted chromaticity values of the measured spectrum. The intersection of this extended line with the curve envelope specifies the *dominant wavelength* λ_{dom} that will be herein considered as the colorimetric definition of the natural water body.

The distinctiveness of this dominant wavelength is termed 'purity'. Spectral purity is a measure of the contribution of the dominant wavelength to an observed optical spectrum. A spectral purity of 1.0 indicates a monochromatic spectrum at the dominant wavelength, λ_{dom}, while a spectral purity p of 0 indicates a 'white' spectrum. Together, the dominant wavelength λ_{dom} and its associated spectral purity p are considered herein as defining aquatic colour.

2.2. *Inverse problem solution*

Pozdnyakov and Lyaskovsky (1999) compared the robustness of several most frequently used algorithms for retrieving water quality parameters in the case of waters ranging from clear to turbid/strongly absorbing. This comparison led to the conclusion that the Levenberg–Marquardt multivariate optimization technique provides the most accurate inverse problem solution in the case of optically complex natural waters, i.e. waters in which phytoplankton, dissolved organics and suspended minerals co-exist largely uncorrelated in substantial amounts. The theoretical foundations and application of this approach have been discussed elsewhere (see e.g. Bukata *et al.* 1995); here we will outline the general concept of this approach.

The formal relation between $L_u(+0, \lambda)$ and $R(\lambda)$ allows the inverse problem solution from $R(\lambda)$.

Considering absorption and elastic scattering, the bulk optical properties of a natural water column, $a(\lambda)$, $b(\lambda)$, $b_b(\lambda)$ can be thought as the sum of the individual IOP of the suspended and/or dissolved organic and/or inorganic materials present in the water column (in addition to the pure water itself). That is:

$$a(\lambda)=\sum_{i=1}^{N} a_i(\lambda),\ b(\lambda)=\sum_{j=1}^{N'} b_j(\lambda),\ b_b(\lambda)=\sum_{j=1}^{N'} b_{bj} \tag{17}$$

where subscripts i and j stand for co-existing absorbing and scattering components, the overall number of which is N and N' respectively.

Introducing *specific* absorption and scattering (backscattering) coefficients, a_i^*, b_j^*, b_{bj}^* at wavelength λ for a unit concentration of aquatic component $i(j)$, the volume reflectance can be presented (equation 1) in vector form (see e.g. Bukata *et al.* 1995):

$$R[\boldsymbol{a}^*(\lambda), \boldsymbol{b}_b^*(\lambda)\boldsymbol{C}] \sim [\boldsymbol{b}_b^*(\lambda).\boldsymbol{C}]/[\boldsymbol{a}^*(\lambda).\boldsymbol{C}] \tag{18}$$

where $\boldsymbol{a}^*(\lambda)=[a_w(\lambda), a_{chl}^*(\lambda), a_{sm}^*(\lambda), a_{doc}^*(\lambda), \ldots]$; $\boldsymbol{b}_b^*(\lambda)=[b_{b_w}(\lambda), b_{b_{chl}}^*(\lambda), b_{b_{sm}}^*(\lambda), 0, \ldots]$; $\boldsymbol{C}=(1, C_{chl}, C_{sm}, C_{doc}, \ldots)$.

If $[S_j]$ is a given spectrum to be processed, consisting of a set of the irradiance reflectance values at discrete wavelengths λ_j, the weighted residuals between $[S_j]$

and modelled irradiance reflectance $R[\boldsymbol{a}^*(\lambda), \boldsymbol{b}_b^*(\lambda)\boldsymbol{C}\}$ can be written as

$$g_i(\boldsymbol{C}) = \{S_j - R[\boldsymbol{a}_j^*, \boldsymbol{b}_{bj}^*, \boldsymbol{C}]\}/S_j \tag{19}$$

The multidimensional least-square solution (at the wavelengths corresponding to $[S_j]$) could be then found through minimizing over the concentration vector $\boldsymbol{C}$ the function of residuals:

$$f(\boldsymbol{C}) = \sum_j g_j^2(\boldsymbol{C}) \tag{20}$$

A search for the function $f(\boldsymbol{C})$ absolute minimum is further carried out utilising the Levenberg-Marquardt finite difference algorithm appropriate for such multivariate non-linear least-squares optimization applications. The result thus obtained can then be interpreted as the desired concentration vector $\boldsymbol{C}$ for the location where the spectrum $[S_j]$ has been recorded. A more detailed description of this method and technology of searching for the absolute minimum of $f(\boldsymbol{C})$ can be found elsewhere (e.g. Kondratyev *et al.* 1990).

A very important advantage of such an approach is that it provides for retrieving *simultaneously* the concentrations of *all* optically active components (OAC) included into the hydrooptical model.

When considering transspectral processes, the inverse problem solution implies in our case both the retrieval (by means of the Levenberg–Marquardt procedure) of the OAC concentration vector from a modelled composite spectrum of $R(\lambda)$, i.e. a spectrum inclusive of contributions from both absorption, elastic scattering, and transspectral interactions, and assessment of the OAC retrieval error arising from neglect of the water Raman and fluorescence by chlorophyll and dissolved organics.

3. Model inputs

Only the nadir (i.e. strictly vertical) viewing direction was considered in all our simulations. Calculations were performed for a calm water surface and the following depth-independent concentrations of OAC: C_{chl} ($\mu g\,l^{-1}$) = 0.0; 0.5; 1.0; 2.0; 3.0; 4.0; 5.0; 15.0, C_{sm} ($mg\,l^{-1}$) = 0.0; 0.5; 1.0; 2.0; 3.0; 4.0; 5.0, C_{doc} ($mgC\,l^{-1}$) = 0.0; 0.5; 1.0; 2.0; 5.0; 10.0. These sets of the OAC concentrations embrace most conditions in natural waters from oligotrophic to meso-eutrophic (Petrova 1990). All calculations were conducted for solar zenith angles equal to 0°, 5°, 10°, 30°, 40°, and 50°.

3.1. *Absorption and elastic scattering*

Equations 1 and 17 indicate that in order to model the spectral distribution of water volume reflectance $R_{e.s.}(\lambda)$, coefficients of specific absorption and backscattering (the latter called otherwise absorption and backscattering cross sections) are required. Such hydrooptical models have been suggested so far in the literature but mostly for clear oceanic waters (see Bukata *et al.* 1995).

Two hydrooptical models have been established for the Great European Lakes (GEL)—Lakes Ladoga and Onega and the Laurential Great Lakes of central North America (Bukata *et al.* 1991). These models include both clear and turbid natural waters, and both proved their validity in a number of independent experiments (Pozdnyakov *et al.* 1999, Bukata *et al.* 1999). In the present study, one of them, *viz.* the GEL model, was used as a basic model for all numerical simulations. This is a four-component model incorporating the spectral values of absorption and backscattering cross sections of water *per se*, phytoplankton, dissolved organics and suspended minerals in the spectral region 410–690 nm in increments of $\Delta\lambda = 20$ nm. The reader

interested in the cross sections tabulated values as well as underlying assumptions and additional details regarding the GEL model is also referred to (Kondratyev *et al.* 1998).

3.2. *Water Raman scattering*

For calculating R_r, formulas (2–9) have been used in accordance with the methodological approach given in section 2. Following equation 2, values are needed for b_r, B_r, μ_d, μ_u, E_d. $b_r(\lambda)$ has been determined by many workers (e.g. see Barlett *et al.* 1998). It lies in the range $(2.7 \pm 0.2) \times 10^{-4}\ \mathrm{m}^{-1}$ at $\lambda = 488$ nm. The spectral dependence of $b_r(\lambda)$ is proportional to λ^{-5} (although it is slightly different for the incident and the Raman scattering wavelengths). The backscattering probability for elastic and inelastic scattering is generally assumed (Marshall and Smith 1990) to be 0.5 due to the known shape of the phase functions (for Rayleigh and isotropic).

The values of $\mu_d(-0, \theta'_0, \lambda)$ were calculated following Berwald *et al.* (1998), μ_u was assumed to be 0.5 bearing in mind the shape of the Raman scattering phase function.

The incident irradiance was simulated in the spectral range 310–690 nm for cloudless sky conditions using the model suggested by Gregg and Carder (1990). The extension of the incident irradiance spectrum into the ultraviolet is due to the Raman frequency shift (~ 75 nm) leading to emissions at $\lambda \geqslant 400$ nm stimulated by photons with $\lambda \geqslant 325$ nm (Sugihara *et al.* 1984).

To calculate K_d (see equation 6), (eventually F_w) as a function of θ_0 and λ is needed; it was taken here from Baker and Smith (1997) for cloudless conditions.

In addition, the backscattering probability for phytoplankton (B_{chl}), suspended minerals (B_{sm}) and water molecules (B_w) needs to be specified to obtain the direct and diffuse light attenuation coefficients (equations 4 and 5). For water, B_w is known to be 0.5 (Morel 1980). For phytoplankton, B_{chl} is reported to be in the range 0.008–0.018 (Siegel *et al.* 1997). We used the value of 0.011, which was recommended by Bukata *et al.* (1995). Data on B_{sm} are scarce. In our simulations B_{sm} was taken to be equal to 0.08 as it was determined for Lake Ontario waters (Bukata *et al.* 1995), which is consistent with the relevant laboratory estimations by Vohen *et al.* (1997). Although it is a rough approximation in the case of phytoplankton, and perhaps also suspended minerals, B values were assumed to be wavelength independent.

Finally, for matching the entire spectral range of the incident radiation (i.e. 310–690 nm), the employed GEL hydrooptical model (basically established for $410 \leqslant \lambda \leqslant 690$ nm) was extended to 310 nm (table 1). In the light of the established phytoplankton UV protection capacities, and arguments given by Kondratyev and

Table 1. Spectral values of the OAC cross sections and water absorption and scattering coefficients in the range 310–410 nm.

λ, nm	a^*_{chl} ($\mathrm{m^2\,mg^{-1}}$)	a^*_{sm} ($\mathrm{m^2\,g^{-1}}$)	a^*_{doc} ($\mathrm{m^2\,(gC)^{-1}}$)	$b^*_{b_{chl}}$ ($\mathrm{m^2\,mg^{-1}}$)	$b^*_{b_{sm}}$ ($\mathrm{m^2\,mg^{-1}}$)	a_w ($\mathrm{m^{-1}}$)	b_w ($\mathrm{m^{-1}}$)
310	0.0350	0.4750	0.5300	0.001435	0.0420	0.1050	0.0176
330	0.0350	0.4250	0.4700	0.001380	0.0407	0.0678	0.0134
350	0.0350	0.3800	0.4150	0.001340	0.0395	0.0463	0.0103
370	0.0355	0.3400	0.3650	0.001305	0.0384	0.0300	0.0081
390	0.0365	0.3000	0.3200	0.001275	0.0374	0.0191	0.0065
410	0.0380	0.2650	0.2800	0.001250	0.0365	0.0162	0.0052

Pozdnyakov (1996), the absorption cross sections were modified as follows: $a^*_{chl}(\lambda)$ was assumed decreasing symmetrically (with respect to the band maximum at ~ 450 nm) until $\lambda = 360$ nm; then in the spectral region 360–310 nm it was held constant at 0.035 $m^2 mg^{-1}$. $a_{doc}(\lambda)$ was extrapolated into the short wavelength region following the exponential law inherent in the visible part of the spectrum (Kirk 1976). Extrapolations of $a_{sm}(\lambda)$, $b_{b\,chl}$ and $b_{b\,sm}$ were conducted according to the power law suggested in Bukata *et al.* (1995). Values of water absorption and scattering coefficients, a_w and b_w, in the range 310–690 nm were taken from Smith and Baker (1981).

3.3. *Fluorescence by chlorophyll and dissolved organics*

The fluorescence models (equations 10 and 13) require, in addition to the adopted hydro-optical model, the following input data: $E_d(\lambda)$, the fluorescence yield for phytoplankton (η_{chl}) and dissolved organics (η_{doc}), Gaussian shape function parameter (σ_{chl}, σ_{doc}), wavelength of maximum fluorescence emission (λ_{0em}) for chlorophyll and dissolved organics.

$E_d(\lambda)$ was simulated as above. The phytoplankton fluorescence yield was assessed by several workers (see e.g. Gordon 1979, Kondratyev *et al.* 1999) and was shown to be strongly dependent on the taxonomic composition of phytoplankton, incident radiation intensity/inhibition, nutrients availability/stress, and some other factors. The published values of η_{chl} vary in a wide range (~ 1–12%) with the most commonly reported numbers from 1–3% (under conditions of maximum photoinhibition). For instance, Babin *et al.* (1996) explored the issue of latitudinal and seasonal distributions of η_{chl} in ocean waters and came to the conclusion that η_{chl} varied between ~ 2.7–4.5% with the maximum values in temperate latitudes. However, according to their estimations, η_{chl} might be much lower ($\sim 1.1\%$) due to a combined action of photoprotectant and nutrient limitation effects. Alongside with these data, there are indications that η_{chl} can be as small as 0.3% (Fischer and Kronfeld 1990). The available data on η_{chl} are generally indicative of a wavelength independence of this physical quantity, which is also a function of the algal species type. In view of all these uncertainties, we have explored, for comparison reasons, two options with $\eta_{chl} = 0.7\%$ and 3% neglecting a wavelength dependence over the entire PAR region.

Although being scarce, the reported data on the fluorescence yield of dissolved organics is nevertheless indicative of a generally strong dependence of η_{doc} on λ. Based on some river water data, it could be assumed that its absolute magnitude varies from about 0.005–0.010 at 250 nm to 0.005–0.019 at 470 nm, with the maximum value ranging between 0.007 and 0.028 at ~ 390 nm (Green and Blough 1994). In our simulations the following spectral values of η_{doc} were employed:

λ (nm)	310	330	350	370	390	410	430	450	470
$\eta_{doc} \times 10^4$	125	175	230	245	270	260	230	210	0

Chlorophyll *a* fluoresces *in vivo* from 660 to 760 nm with the principal maximum at ~ 685 nm. (see Gordon 1979). Due to an extremely complex and water body-dependent chemical composition, dissolved organics exhibit less rigid boundaries of emission spectra, ranging from about 400 nm to 620–660 nm and peaking at 490–510 nm (Vodacek *et al.* 1994). However, Coble and Brophy (1996) found that the dissolved organics fluorescence maximum is located at somewhat lower wavelengths.

In conformity with these data, the emission band shape was represented by a Gaussian function centred at 685 nm for chlorophyll and 490 nm for dissolved organics with the widths at half-maximum of about 25 nm and $\sim$100 nm respectively.

The GEL model was used in its spectrally extended form as described above. In applying equations 10 and 13, it was assumed that $a_f \equiv a_{chl}$ or a_{doc}. If in the case of chlorophyll this assumption is easily justifiable, but it appears less warranted for dissolved organics. Indeed, there are indications (Kondratyev *et al.* 1999) that only a certain proportion of dissolved organics is fluorescent. However, being unaware of any data on this score, we assumed identity between a_f and a_{doc}. The integration in equations 10 and 13 was performed over the entire spectral region (i.e. 310–690 nm).

3.4. *Radiometric water colour*

Simulations of radiometric water colour were performed based on equations 14–16. As defined in §2.1, λ_{dom} and p were used as radiometric colour parameters. As input parameters, $E_d(+0, \lambda)$, the GEL model for the visible spectrum, the CIE colour mixtures for equal energy spectra, solar zenith angle, $\theta_0 = 30^\circ$ and the relative index of refraction of water to air, $n = 1.341$ were exploited. $E_d(+0, \lambda)$ was obtained using the model suggested by Gregg and Carder (1990). The CIE colour mixtures for equal energy spectra were taken from CIE tables (Anonymous 1957).

4. Forward modelling results

4.1. *Water Raman scattering*

Our computational results on spectral variations of the upwelling irradiance, $E_u^r(-0, \lambda)$, arising from pure water Raman scattering ($C_{chl} = C_{sm} = C_{doc} = 0$), indicate that $E_u^r(-0, \lambda)$ increases with λ reaching a maximum at $\sim$430–470 nm which is then followed by a steep fall-off at longer wavelengths. Haltrin and Kattawar (1993) reported a very similar result. This pattern of spectral variations of $E_u^r(-0, \lambda)$ is mostly due to a concerted impact of three factors: (a) the incident radiation, strongly reduced in the short wavelength region, shows a rather broad maximum at about 480–490 nm, and a fall-off at $\lambda > 490$ nm); (b) b_{b_r} is being proportional to $\sim\lambda^{-5}$; and (c) attenuation coefficients K_u, K_d increase for $\lambda > 490$ nm). However, the contribution of Raman scattering to the water-leaving radiance exhibits a different behaviour: it progressively increases with λ, and reaches $\sim$20% at $\lambda \geqslant 650$ nm. This value is very close to the figures ($\sim$19–21%) reported in the literature (Waters 1995), and results mostly from the Raman frequency shift ($\geqslant$75 nm).

Calculations for varying solar zenith angle θ_0 give a weak growth of the Raman scattering contribution to $E_u(-0, \lambda)$ with increasing θ_0 for $\lambda \leqslant 520$ nm. At the same time, the proportion of $E_u^r(-0, \lambda)$ in the resultant upwelling radiance decreases with increasing θ_0 in the yellow to red portions of the spectrum. These results comply well with those reported by Waters (1995).

The dependence on sun zenith angle described above is inherent in an increase of the photon path length in the water, and hence in an increase in the photon absorption probability which is known (Jerlov 1976) to grow with decreasing λ in the spectral region ($\lambda < 400$ nm) and increasing λ in the range yellow–red.

Addition of either phytoplankton or suspended minerals or dissolved organics to pure water results in a substantial decrease in $E_u^r(-0, \lambda)$ at wavelengths > 500 nm. Waters (1995) reports similar behaviour of $E_u^r(-0, \lambda)$ with increasing phytoplankton concentration in a two-component (pure water–phytoplankton) system. This effect is due to the ability of the above OAC to absorb light in the short wavelength

region, and it proves to be most accentuated in the case of dissolved organics whose absorptivity increases exponentially with decreasing λ.

Figure 1 illustrates the relevant spectral variations of total volume reflectance (i.e. volume reflectance composed of $R_{e.s.}$ and R_r) at $\theta_0 = 10^\circ$ for three modelling options: pure water plus phytoplankton (figure 1(*a*)), pure water plus suspended minerals (figure 1(*b*)), and pure water plus dissolved organics (figure 1(*c*)). Increasing amounts of each of these constituents of natural water reduce the resultant volume reflectance down to the $R_{e.s.}$ value (table 2), thus indicating that even at high solar zenith angles the contribution of Raman scattering to the volume reflectance in moderately to strongly turbid/absorbing waters is only small at all wavelengths.

The relative contribution of R_r to the total volume reflectance slightly decreases with increasing θ_0 mostly as a result of two reasons. Firstly, it is known (Gordon 1989) that $R_{e.s.}(-0, \lambda)$ increases with increasing θ_0. Secondly, as we saw here, the contribution of $E_u^r(-0, \lambda)$ to $E_u(-0, \lambda)$ decreases with increasing θ_0. The spectral variations of this dependence are illustrated in both figure 2 and table 3.

4.2. *Fluorescence by chlorophyll and dissolved organics*

The use of both fluorescence models (equations 10 and 13) for the calculation of relative contributions to volume reflectance reproduced earlier results for single fluorescence models. Figures 3 and 4 illustrate the results for a variety of hydrooptical conditions. In compliance with other studies and measurements, the spectral region within which the resultant volume reflectance is affected by fluorescence proved to be >660 nm for chlorophyll and $\sim(430–660)$ nm for dissolved organics. Culver and Perry (1997) report that solar-induced chlorophyll *a* fluorescence accounts for 10–40% of the total upwelling irradiance at the surface. Vodacek *et al.* (1994) report that the dissolved organics fluorescence contribution to the reflectance in the blue-green to green spectral region can be as high as 70% for black water (i.e. water without suspended sediments and phytoplankton). These two assessments compare well with our results illustrated in figure 5, which also shows the dependence of the fluorescence contribution to total volume reflectance on solar zenith angle. However, the curves in figures 3 and 4 clearly indicate a strong sensitivity of R^f (both in the case of chlorophyll and dissolved organics fluorescence) to the presence of absorbing and/or scattering matter: R^f rapidly decreases as OAC concentrations grow. Suspended minerals prove to be especially efficient in damping the fluorescence-driven volume reflectance. Therefore, the impact of transspectral processes on the upwelling irradiance (radiance) can be expected to be very low in strongly absorbing/scattering waters. However, obviously it is not the case for *moderately* absorbing/scattering waters.

A fluorescence 'signal' in the spectral distribution of volume reflectance can be detected in waters rich either in phytoplankton or dissolved organics but containing only small amounts of suspended minerals.

We believe that we have experimental evidence of the impact of dissolved organics fluorescence on $R(-0, \lambda)$. Concurrent measurements of OAC concentrations and subsurface upwelling and downwelling irradiances (at SeaWiFS wavelengths: 412, 443, 490, 510, 555, 670 nm) were conducted in Saginaw Bay (Pozdnyakov *et al.* 1999). From prospective of trophic conditions, Saginaw Bay is generally subdivided into two parts, the inner and outer parts. The former is eutrophic, and the latter is oligotrophic. Importantly, being relatively deficient in phytoplankton and suspended minerals, waters in the outer part are rather rich in dissolved organics, and thus

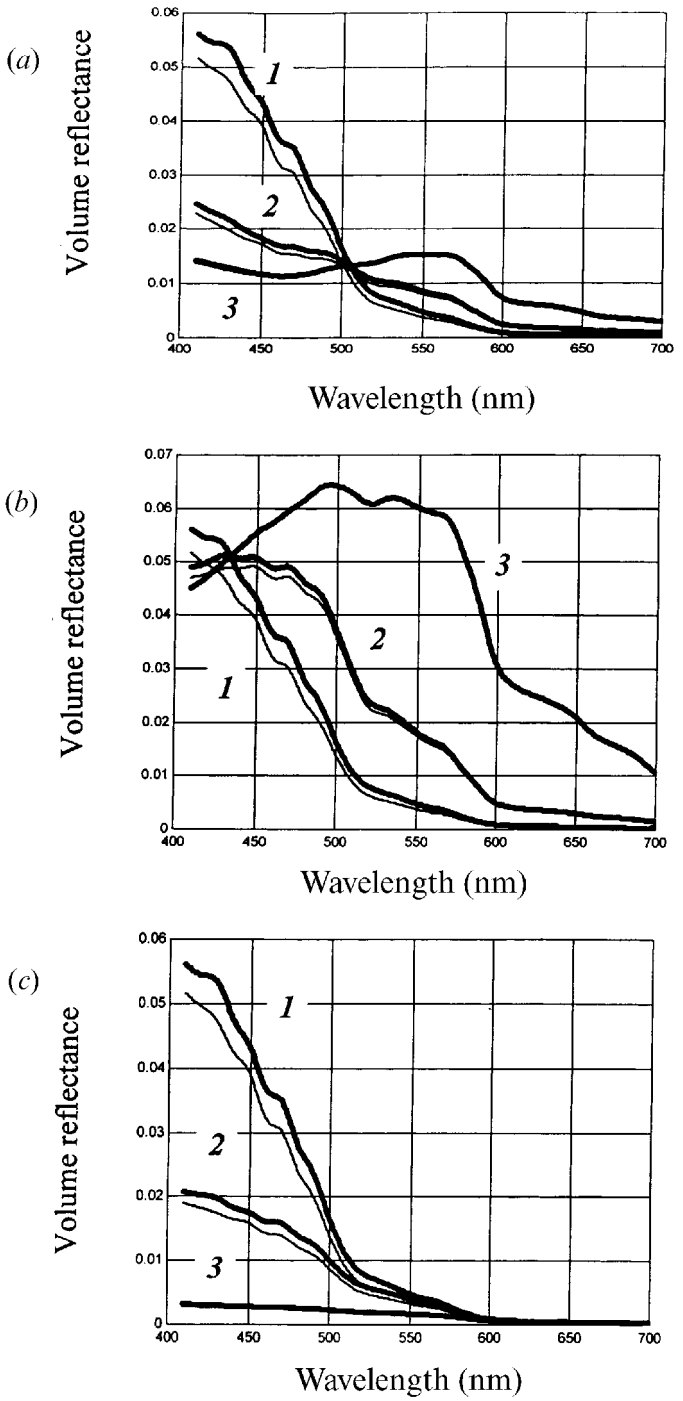

Figure 1. Impact of water Raman scattering on the volume reflectance for a number of hydro-optical options. (*a*) $C_{sm} = C_{doc} = 0$, graph 1: $C_{chl} = 0$; graph 2: $C_{chl} = 1.0$; graph 3: $C_{chl} = 5.0\ \mu g l^{-1}$, (*b*) $C_{chl} = C_{doc} = 0$; graph 1: $C_{sm} = 0$; graph 2: $CD_{sm} = 0.1\ mg l^{-1}$; graph 3: $C_{sm} = 1.0\ mg l^{-1}$, (*c*) $C_{sm} = C_{chl} = 0$, graph 1: $C_{doc} = 0$; graph 2: $C_{doc} = 0.1\ mgC l^{-1}$; graph 3: $C_{doc} = 1.0\ mgC l^{-1}$. Solar zenith angle $\theta_0 = 10^\circ$. Thin lines refer to $R_{e.s.}$ only.

Table 2. Relative contribution to spectral volume reflectance from water Raman scattering for a variety of hydro-optical options at $\theta_0 = 10°$. Concentrations of chlorophyll, suspended minerals and dissolved organics are given in $\mu g\,l^{-1}$, $mg\,l^{-1}$, and $mgC\,l^{-1}$ respectively. Fluorescence effects due to chlorophyll and dissolved organics are neglected.

	Options					
	$C_{sm} = C_{doc} = 0$		$C_{chl} = C_{doc} = 0$		$C_{chl} = C_{sm} = 0$	
λ (nm)	$C_{chl} = 1$	$C_{chl} = 5$	$C_{sm} = 0.1$	$C_{sm} = 1$	$C_{doc} = 0.1$	$C_{doc} = 1$
400	0.08	0.04	0.05	0.01	0.1	0.11
500	0.07	0.02	0.04	0.00	0.11	0.04
650	0.07	0.02	0.04	0.00	0.26	0.22

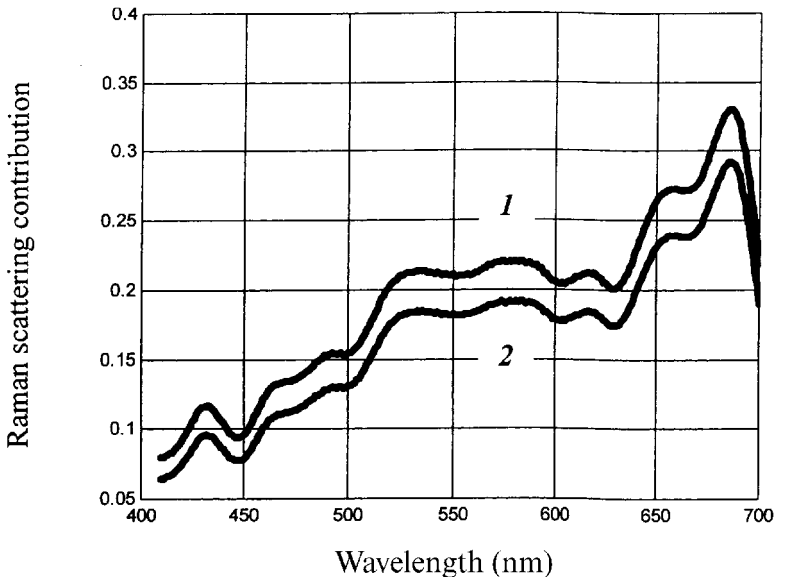

Figure 2. Pure water Raman scattering contribution to the volume reflectance $R(-0, \lambda)$ for two solar zenith angles: graph 1: 10°; graph 2: 45°.

Table 3. Relative contribution to spectral volume reflectance from water Raman scattering for two sun zenith angles in the case of pure water ($C_{chl} = C_{sm} = C_{doc} = 0$).

	θ_0 (°)	
λ (nm)	10	45
400	0.09	0.07
500	0.15	0.13
650	0.26	0.23

constitute favourable conditions for detection of the dissolved organics fluorescence signal in $R(-0, \lambda)$. Indeed, more than 20 determinations of $R(-0, \lambda)$ in the outer part of Saginaw Bay revealed under varying sun illumination conditions

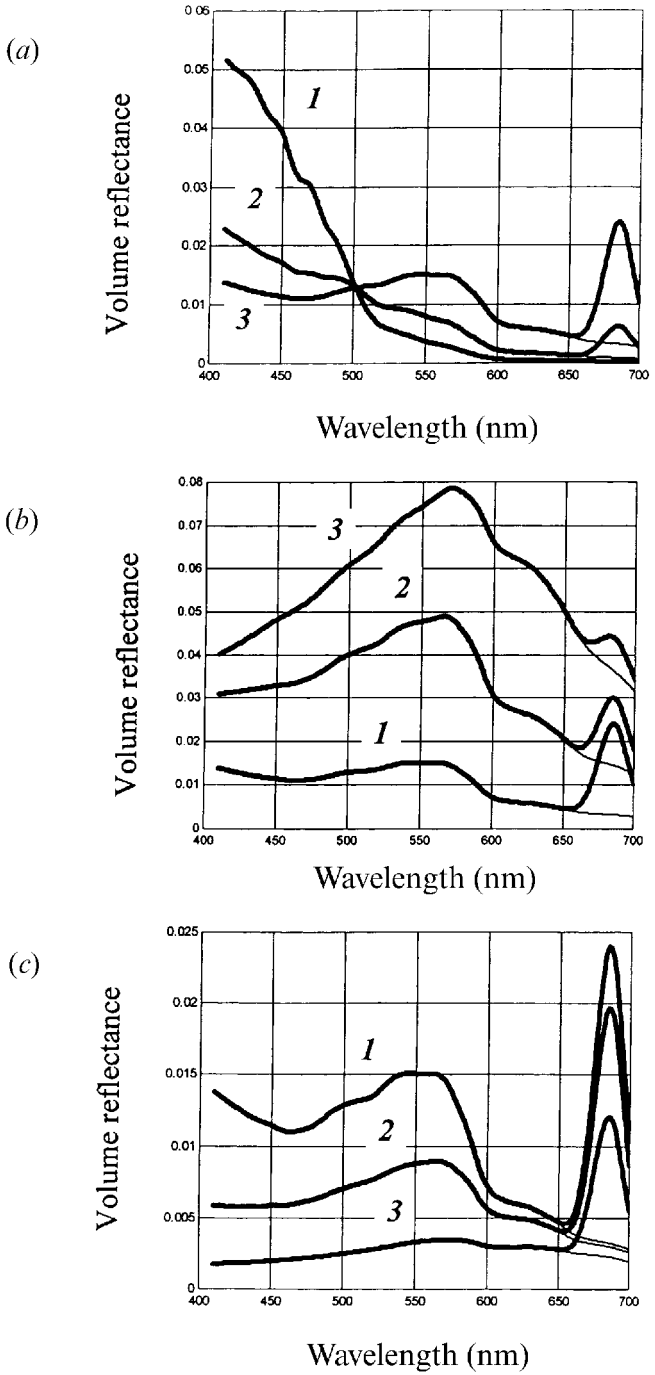

Figure 3. Chlorophyll fluorescence impact ($\eta_{chi} = 3\%$) on the volume reflectance $R(-0, \lambda)$ for a number of hydro-optical options. (*a*), $C_{sm} = C_{doc} = 0$, graph 1: $C_{chl} = 0$; graph 2: $C_{chl} = 1.0\,\mu g\,l^{-1}$; graph 3: $C_{chl} = 5.0\,\mu g\,l^{-1}$, (*b*) $C_{chl} = 5\,\mu g\,l^{-1}$; $C_{doc} = 0$; graph 1: $C_{sm} = 0$; graph 2: $C_{sm} = 1.0\,mg\,l^{-1}$; graph 3: $C_{sm} = 5.0\,mg\,l^{-1}$, (*c*) $C_{sm} = 0$, $C_{chl} = 5\,\mu g\,l^{-1}$, graph 1: $C_{doc} = 0$; graph 2: $C_{doc} = 1.0\,mgC\,l^{-1}$; graph 3: $C_{doc} = 5.0\,mgC\,l^{-1}$. Solar zenith angle $\theta_0 = 10^\circ$. Thin lines refer to $R_{e.s.}$ only.

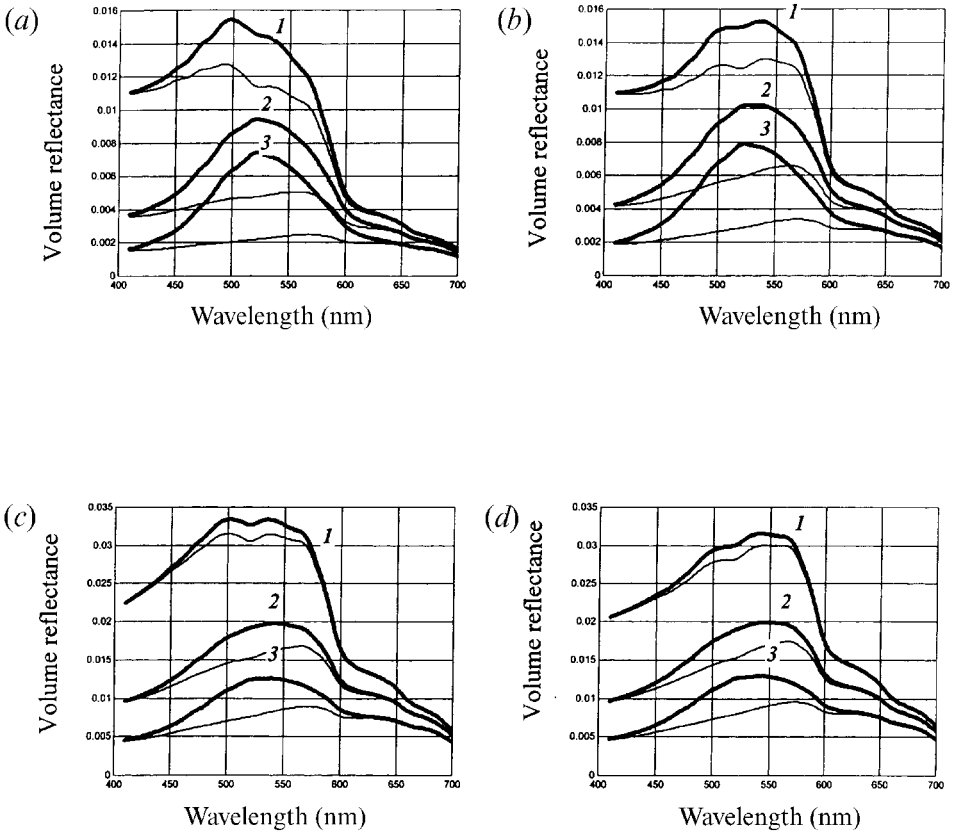

Figure 4. Dissolved organics fluorescence impact ($\eta_{doc}(\lambda)$ is as given in the input data section) on the volume reflectance $R(-0, \lambda)$ for a variety of OAC concentration vectors. (*a*) $C_{chl} = 0.5\,\mu g\,l^{-1}$, $C_{sm} = 0.1\,mg\,l^{-1}$; (*b*) $C_{chl} = 2.0\,\mu g\,l^{-1}$, $C_{sm} = 0.1\,mg\,l^{-1}$; (*c*) $C_{chl} = 0.5\,\mu g\,l^{-1}$, $C_{sm} = 0.5\,mg\,l^{-1}$; (*d*) $C_{chl} = 2.0\,\mu g\,l^{-1}$, $C_{sm} = 0.5\,mg\,l^{-1}$; $C_{doc} = 0.5\,mgC\,l^{-1}$. Graph 1: $2.0\,mgC\,l^{-1}$; graph 2: $5.0\,mg\,l^{-1}$; graph 3: Solar zenith angle $\theta_0 = 10°$. Thin lines refer to $R_{e.s.}$ only.

($22° < \theta_0 < 50°$) and wind force (calm÷ $5\,m\,s^{-1}$) a maximum at $\sim$490 nm and an inflection at 555 nm. Figure 6 (curve 1) illustrates such a spectrum for one of the stations. The concentrations of chlorophyll, suspended minerals and dissolved organics determined *in situ* at this station proved to be $1.13\,\mu g\,l^{-1}$, $0.14\,mg\,l^{-1}$ and $1.14\,mgC\,l^{-1}$. The solar zenith angle at the moment of measurements was 30°. Several hydro-optical models were tested to simulate the experimental spectrum of $R(-0, \lambda)$. The best fit was attained (figure 6, curve 2) with the Ontario Lake model (Bukata *et al.* 1991). However, even this model failed to reproduce the main maximum at $\sim$490 nm. The inclusion of the dissolved organics and chlorophyll fluorescence impact on $R(-0, \lambda)$ using the above methodology and η_{doc} as in the input data section, and $\eta_{chl} = 0.7\%$ resulted in a good match between the measured and simulated $R(-0, \lambda)$ spectra (Pozdnyakov *et al.* 2000). Thus, this evaluation seems to provide evidence of the actual manifestation of dissolved organics fluorescence in natural waters.

This is further substantiated by the data obtained in the course of the same field campaign: the spectral feature in $R(-0, \lambda)$ at $\sim$490 nm gradually declines and turns

into an inflexion, as the stations are nearer the inner part of the bay, and the water is relatively more abundant in chlorophyll and suspended minerals. Inside the inner bay, spectra of $R(-0, \lambda)$ do not display any specific feature at ~ 490 nm. Disappearing completely, this feature gives way to very low (about 1% and less) values of $R(-0, \lambda)$ in the spectral region 400–530 nm with the maximum of $R(-0, \lambda)$ (about 3%) at ~ 560 nm.

Given the typical concentrations of OAC observed in the inner part of the bay ($C_{chl} \geqslant 10\ \mu g\,l^{-1}$, $C_{sm} = 2 \div 3\ mg\,l^{-1}$, $C_{doc} \sim 3\ mgC\,l^{-1}$), the disappearance in the simultaneously measured $R(-0, \lambda)$ spectra of the spectral feature at 490 nm seems to corroborate our forward modelling results. Indeed, as shown above, the fluorescence signal due to dissolved organics is most pronounced in the spectrum of $R(-0, \lambda)$ when the water is nearly devoid of chlorophyll and suspended minerals. Enrichment of water with chlorophyll and suspended minerals (at a given C_{doc}) results in a rapid deterioration of expression of dissolved organics fluorescence in the $R(-0, \lambda)$ spectral distribution (figure 4a and 4d). Thus, with chlorophyll and suspended minerals increasing along the axis extending from the outer part to the inner part of the bay, the expression of dissolved organics fluorescence in $R(-0, \lambda)$ first transforms from a maximum to an inflexion and then disappears completely becoming masked by the predominant impact of absorption of both chlorophyll and suspended minerals (for more details see Pozdnyakov *et al.* 2000).

Finally, in support of the suggested interpretation of the Saginaw Bay spectral data and our numerical modelling results it is worth mentioning that analogous spectral distributions of $R(-0, \lambda)$ exhibiting either a maximum or inflexion at ~ 490 nm have been recorded in some small (sometimes, nearly pristine) lakes in northern Ontario in the cases when dissolved organics proved to be relatively high whereas chlorophyll and suspended minerals were present in low amounts (Tanis 1999, personal communication).

4.3. *Radiometric water colour*

Based on numerical simulations using the methodology discussed above and hydrooptical models of Lakes Ladoga and Ontario, Bukata *et al.* (1997) analysed radiometric colour response to the OAC concentration vector variations. The major results of these studies are summarized below (Bukata *et al.* 1999):

1. Natural waters that contain simultaneously low concentrations of chlorophyll, suspended minerals, and dissolved organics appear blue to turquoise in colour (dominant spectral wavelength λ_{dom} in the range 472 nm–500 nm).
2. Highly turbid waters (i.e. waters containing high concentrations of chlorophyll and/or suspended minerals) display colours ranging from green to brown (i.e. $\lambda_{dom} > 500$ nm).
3. Waters with high concentrations of dissolved organics, irrespective of turbidity, are invariably perceived as brownish (λ_{dom} in the range 560 nm–570 nm), unless the concentrations of chlorophyll and suspended minerals are infinitesimally low (in the latter case λ_{dom} remains nearly invariant and equal to ~ 480 nm provided $C_{doc} \geqslant 0.5\ mgC\,l^{-1}$).
4. Increasing the OAC content of *all* natural waters, either individually or collectively, results in an asymptotic approach to an 'end-point' dominant wavelength at about 572 nm, an 'end-point' colour physically located in the yellow-green region of the visible spectrum.

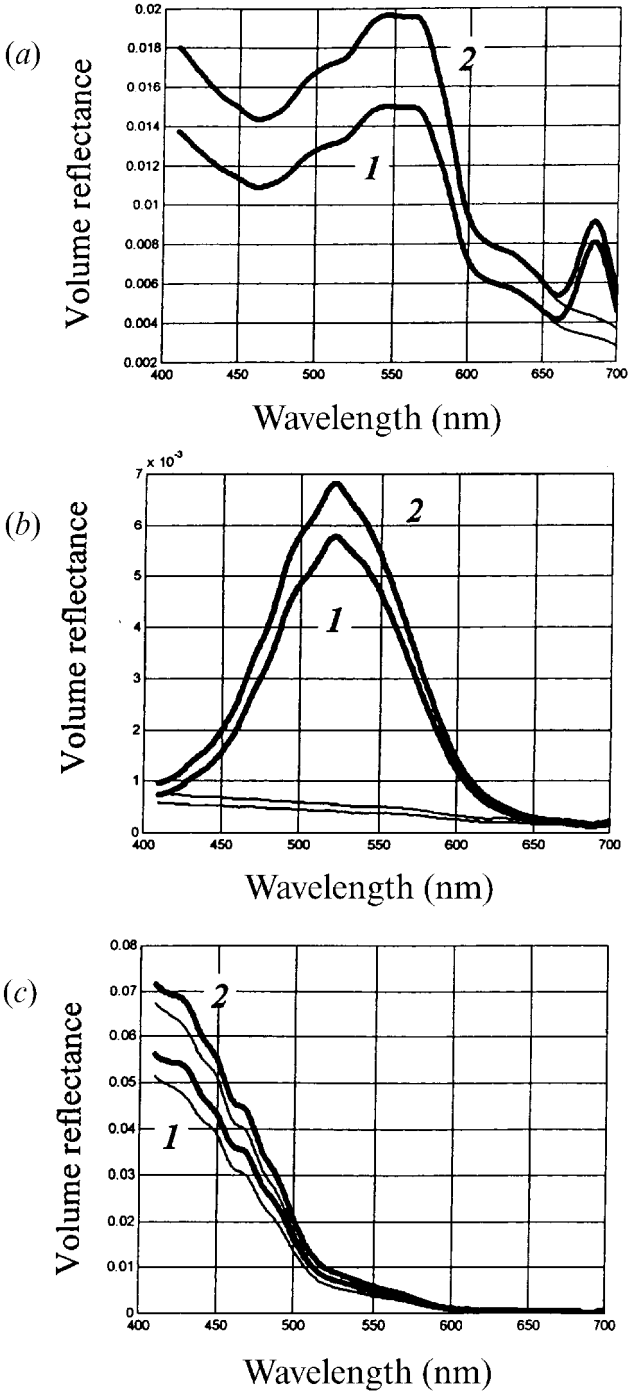

Figure 5. The influence of sun zenith angle on the volume reflectance $R(-0, \lambda)$ including fluorescence and water Raman scattering. (*a*) $C_{chl} = 5\,\mu g\,l^{-1}$, $C_{sm} = C_{doc} = 0$; (*b*) $C_{chl} = C_{sm} = 0$, $C_{doc} = 5\,mgC\,l^{-1}$; (*c*) $C_{chl} = C_{sm} = C_{doc} = 0$; Thin lines refer to $R_{e.s.}$ only. $\eta_{chl} = 0.7\%$, $\eta_{doc}(\lambda)$ is as given in the input data section. Solar zenith angles – graph 1: 5°; graph 2: 50°.

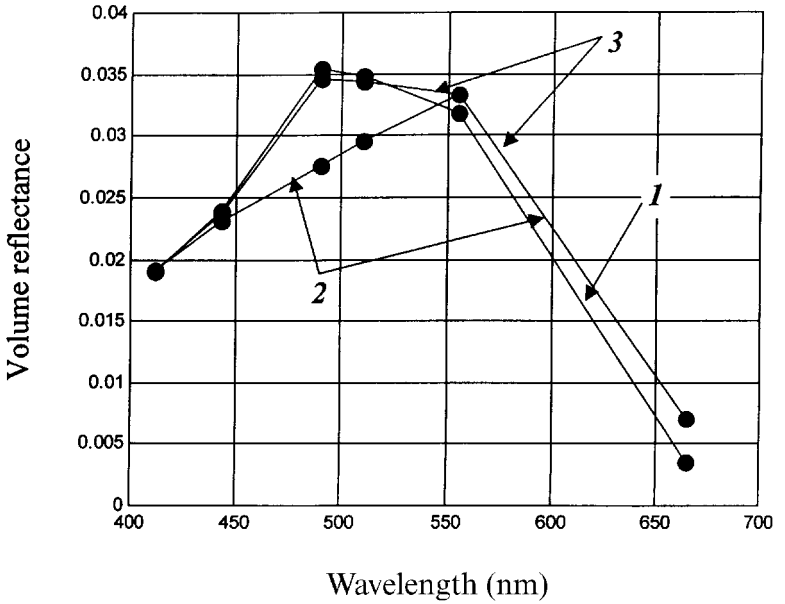

Figure 6. Comparison of $R(-0, \lambda)$ determined at one of the stations in the outer part of Saginaw Bay (graph 1) with the spectra reconstructed with (graph 3) and without (graph 2) consideration of the fluorescence of dissolved organics.

5. When one or more OAC exceeds a critical concentration, the spectral purity p of the 'end-point' colour asymptotically approaches values in the range 0.35–0.45.
6. The intrinsic characteristic yellow-green 'end-point' colour of all natural waters with increasing OAC, coupled with a low spectral distinctiveness (low 'end-point' purity) of this yellow-green colour results in the perceived 'end-point' colour of all natural water bodies appearing brownish in colour.

The consideration of fluorescence by dissolved organics and phytoplankton chlorophyll proved to be conducive to substantial departures from the above generalities. In the first place, the aforementioned irresponsiveness of λ_{dom} to increasing amounts of dissolved organics (beyond a certain threshold of C_{doc}) at very low concentrations of chlorophyll ($<0.2\,\mu g l^{-1}$) and suspended minerals ($<0.1\,mg l^{-1}$) is lost at least at $C_{doc} \leqslant 10\,mgC l^{-1}$ (figures 7 and 8, computations for $\theta_0 = 30°$, $\eta_{chl} = 0.7\%$).

In addition, the common 'end-point' colour at large concentrations of OAC no longer exist in the range $0 < C_{doc} \leqslant 10\,mgC l^{-1}$, when the fluorescence impacts are included. Rather, this common 'end-point' colour becomes concentration vector-specific. Importantly, the dominant wavelengths corresponding to these specific 'end-point' colours are generally substantially shorter (unless $C_{sm} \geqslant 5\,mg l^{-1}$) than the 'end-point' λ_{dom} in the 'absence' of fluorescence (i.e. 560 nm–570 nm). This is especially so when the water turbidity is controlled exclusively by phytoplankton (i.e. $C_{sm} = 0$), e.g. λ_{dom} of the 'end-point' colour at $C_{chl} = 10\,\mu g l^{-1}$ is <550 nm as compared to ~ 570 nm when the fluorescence impact is neglected (figures 7 and 8).

With increasing c_{chl}, the chlorophyll fluorescence causes a more rapid approach

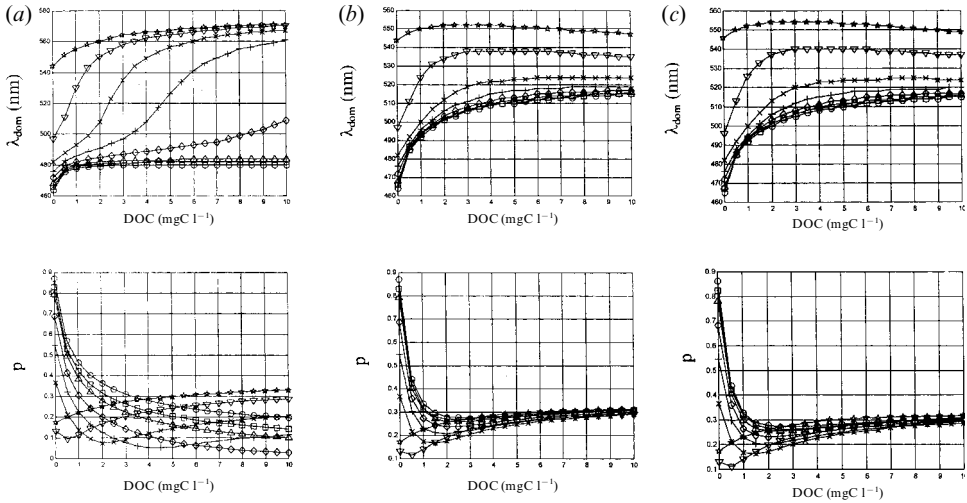

$C_{chl}(\mu g\ l^{-1})$: 0 (O), 0.1 (□), 0.2 (Δ), 0.5 (◊), 1 (+), 2 (×), 5 (▽), 10 (☆)

Figure 7. Variations of the dominant wavelength λ_{dom} and colour purity p in water devoid of suspended minerals when the impacts due to fluorescence of dissolved organics and chlorophyll are neglected (*a*) and taken into consideration (*b*, *c*). *b*: only dissolved organics fluoresce; *c*: both dissolved organics and chlorophyll fluoresce. $\eta_{chl} = 0.7\%$, $\eta_{doc}(\lambda)$ is as given in the input data section, $\theta_0 = 30^\circ$.

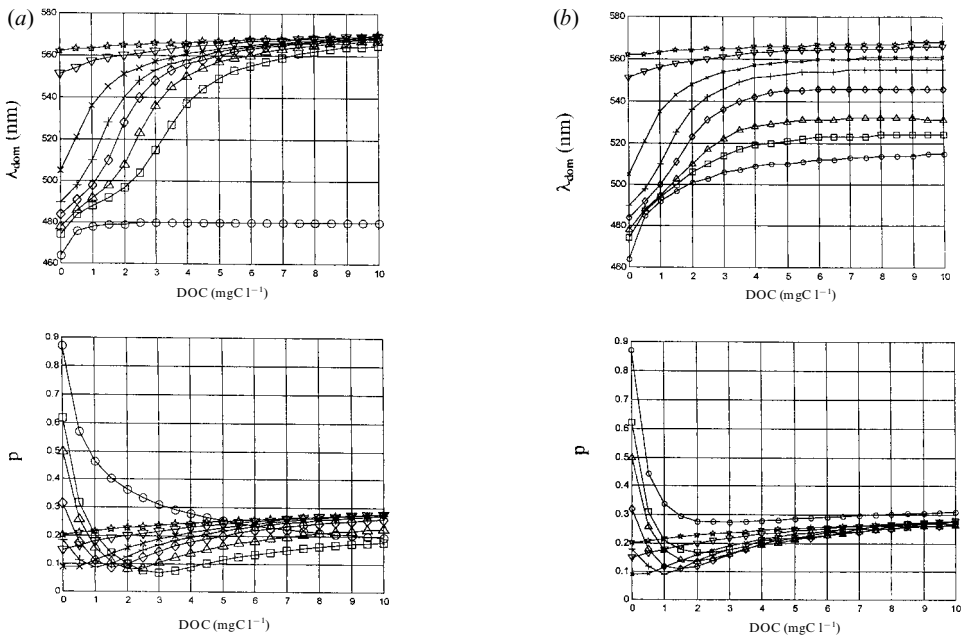

$C_{sm}(mg\ l^{-1})$: 0 (O), 0.1 (□), 0.2 (Δ), 0.5 (◊), 1 (+), 2 (×), 5 (▽), 10 (☆)

Figure 8. Variations of the dominant wavelength and colour purity in water devoid of chlorophyll when the fluorescence of dissolved organics is neglected (*a*) or taken into consideration (*b*). $\eta_{chl} = 0.7\%$, $\eta_{doc}(\lambda)$ is as given in the input data section, $\theta_0 = 30^\circ$. C_{sm} (mg/l): 0 (○), 0.1 (□), 0.2 (△), 0.5 (*), 1 (+), 2 (×), 5 (▽), 10 (☆).

to the 'end-point', although at smaller λ_{dom}. This 'end-point' shifting to shorter wavelengths proves to be nearly independent of η_{chl}.

As seen from figures 7 and 8, contrary to the behaviour of λ_{dom}, the asymptotic approach of colour purity p to values in the range 0.35–0.45 (when one or more CPA exceeds a critical concentration) becomes more rapid with due account of fluorescence effects.

In summary, simulations using widely accepted relations between OAC concentrations on one side and optical properties and fluorescence on the other side show that fluorescence mechanisms influence the colour of natural water bodies, especially when the concentration of one of the fluorophores is relatively high whereas the other OAC are in low quantities. This conclusion is supported by the data from Saginaw Bay. For instance, at a station with $C_{chl} = 1.13\,\mu g l^{-1}$, $C_{sm} = 0.14\,mg l^{-1}$, $C_{doc} = 1.14\,mgC l^{-1}$ in the outer part of Saginaw bay λ_{dom} was equal to 501 nm, but becomes 525 nm after subtraction of the dissolved organics fluorescence signal. As it could be anticipated from above, the colour purity p undergoes only minor changes from 0.09 to 0.08 for this case.

5. Retrieval of water constituents from water colour data

Volume reflectance spectra accounting for the fluorescence by chlorophyll and dissolved organics have been calculated in our study for many sets of OAC concentrations (table 4). These spectra were then subjected to the Levenberg–Marquardt procedure to retrieve C_{chl}, C_{doc} and C_{sm} with the purpose of exploring the impact of fluorescence on the retrievals.

Table 4 indicates that the retrieval accuracy is high for low chlorophyll fluorescence yield. Naturally, the same applies to $\eta_{doc}(\lambda)$. This result is obvious if the fluorescence-driven contributions to volume reflectance are considered as perturbations to the input parameters within the Levenberg–Marquardt retrieval procedure, which are the measured/determined spectrum of R, and/or the applied hydro-optical model. Indeed, it was shown (Pozdnyakov and Lyaskovsky 1999) that as soon as these perturbations are in excess of $\sim 5\%$, the retrieval accuracy dilapidates dramatically.

Tables 5–8 (calculated for $\theta_0 = 30^\circ$) display the retrieval errors $\Delta C_{doc} = (C_{doc}^{input} - C_{doc}^{retrieved})/C_{doc}^{input}$, $\Delta C_{sm} = (C_{sm}^{input} - C_{sm}^{retrieved})/C_{sm}^{input}$, $\Delta C_{chl} = (C_{chl}^{input} - C_{chl}^{retrieved})/C_{chl}^{input}$, induced by the influence of fluorescence on the upwelling radiance (C_i^{input} is the concentration of an optical constituent, used in the calculations).

For the assumed $\eta_{doc}(\lambda)$ and $\eta_{chl} = 0.7\%$, the retrieval error ΔC_{doc} in the case of water devoid of phytoplankton and suspended minerals is always positive increasing up to $\sim 57\%$ at $C_{doc} = 10\,mgC l^{-1}$ (table 5).

Addition of chlorophyll ($\leqslant 5\,\mu g l^{-1}$) results in a rapid decrease of ΔC_{doc} to 20% and even less (table 6). However, a further growth of chlorophyll content leads to overestimation of C_{doc}, and exceeds 50% at $C_{chl} = 15\,\mu g l^{-1}$. Additionally, these variations of ΔC_{doc} change strongly if water contains not only chlorophyll but also suspended minerals. For $C_{chl} \leqslant 5\,\mu g l^{-1}$, the addition of suspended minerals enhances the ΔC_{doc} reduction, whereas for $C_{chl} > 5\,\mu g l^{-1}$, the effect is opposite, i.e. ΔC_{doc} decreases with increasing concentrations of both chlorophyll and suspended minerals.

The error in the retrieval of C_{chl} increases with C_{doc}, but ΔC_{chl} is strongly dependent on the concentration of suspended minerals: the more suspended minerals, the lower ΔC_{chl} (table 7).

Also, the C_{sm} retrieval accuracy depends on the fluorescence of chlorophyll and dissolved organics. For $C_{chl} \leqslant 5\,\mu g l^{-1}$ and $C_{doc} \leqslant 2\,mgC l^{-1}$, ΔC_{sm} can be both positive

Table 4. Impact of Raman scattering, chlorophyll fluorescence and dissolved organics fluorescence on the OAC retrieval results (in round figures) for some combinations of OAC concentrations, $\theta_0 = 30^\circ$, and chlorophyll fluorescence quantum yields 0.7% and 3%.

OAC vector identification	CHL ($\mu g l^{-1}$)		SM ($mg l^{-1}$)		DOC ($mgC l^{-1}$)	
	$\eta_{chl} = 0.7\%$	$\eta_{chl} = 3\%$	$\eta_{chl} = 0.7\%$	$\eta_{chl} = 3\%$	$\eta_{chl} = 0.7\%$	$\eta_{chl} = 3\%$
Input OAC vector	5		0		0	
Retrieved OAC vector	6.0	4.3	0.0	0.5	0.1	1.8
Input OAC vector	5		0		0.1	
Retrieved OAC vector	6.5	2.5	0.0	0.6	0.1	2.7
Input OAC vector	5		0		1	
Retrieved OAC vector	5.3	0.4	0.1	0.1	1.3	5.6
Input OAC vector	5		0		2	
Retrieved OAC vector	0.7	2.8	0.2	4.7	2.4	0.0
Input OAC vector	5		0		5	
Retrieved OAC vector	0.0	15.1	0.3	0.3	4.5	11.0
Input OAC vector	0		5		0	
Retrieved OAC vector	0.4	0.2	5.3	5.8	0.0	0.2
Input OAC vector	5		0.1		0	
Retrieved OAC vector	5.2	5.5	0.2	0.5	0.1	1.0
Input OAC vector	5		1		0	
Retrieved OAC vector	4.7	5.1	1.1	1.5	0.1	0.3
Input OAC vector	5		2		0	
Retrieved OAC vector	5.1	5.0	2.1	2.6	0.0	0.3
Input OAC vector	5		5		0	
Retrieved OAC vector	4.4	5.0	5.1	5.9	0.1	0.2
Input OAC vector	5		2		0.1	
Retrieved OAC vector	5.0	5.0	2.1	2.6	0.1	0.4
Input OAC vector	5		2		1	
Retrieved OAC vector	4.6	4.1	2.1	2.6	1.0	1.6
Input OAC vector	5		2		2	
Retrieved OAC vector	4.5	3.3	2.1	2.6	2.0	2.7
Input OAC vector	5		2		5	
Retrieved OAC vector	0.5	1.0	2.1	2.5	5.0	5.5
Input OAC vector	0		0		0.1	
Retrieved OAC vector	0.1	0.1	0.0	0.0	0.1	0.1
Input OAC vector	0		0		1	
Retrieved OAC vector	0.2	0.2	0.0	0.0	0.9	0.9
Input OAC vector	0		0		2	
Retrieved OAC vector	0.2	0.2	0.0	0.0	1.3	1.3
Input OAC vector	0		0		5	
Retrieved OAC vector	0.0	0.0	0.0	0.0	2.5	2.5

Table 5. Retrieval error, ΔC_{doc}, originating from the fluorescence of dissolved organic ($v_{doc}(\lambda)$ is as given in the input data section), $C_{chl} = C_{sm} = 0$.

	C_{doc} ($mgC l^{-1}$)				
	0.5	1.0	2.0	5.0	10.0
ΔC_{doc}	0.27	0.34	0.41	0.51	0.57

Table 6. Retrieval error, ΔC_{doc}, originating from the fluorescence of dissolved organic and phytoplankton ($\eta_{doc}(\lambda)$ is as given in the input data section), $C_{doc}^{input} = 2\,\mathrm{mgC\,l^{-1}}$.

			Cchl ($\mu\mathrm{g\,l^{-1}}$)						
	η_{chl} (%)	C_{sm} ($\mathrm{mg\,l^{-1}}$)	0.5	1.0	2.0	3.0	4.0	5.0	15.0
ΔC_{doc}	0.7	0.5	0.23	0.13	−0.04	−0.07	−0.10	−0.13	−0.53
		1.0	0.12	0.09	−0.01	−0.02	−0.04	−0.07	−0.37
		2.0	0.11	0.04	0.03	0.01	−0.01	−0.03	−0.24
		3.0	0.14	0.04	0.03	0.02	0.01	−0.05	−0.18
		4.0	0.16	0.05	0.03	0.02	0.01	−0.00	−0.15
		5.0	0.18	0.05	0.04	0.03	0.01	0.00	−0.12
	3.0	0.5	0.09	0.05	−0.22	−0.45	−0.68	−0.89	−4.48
		1.0	0.09	0.00	−0.16	−0.28	−0.42	−0.56	−3.07
		2.0	0.10	0.00	−0.08	−0.16	−0.25	−0.34	−1.98
		3.0	0.11	0.00	−0.06	−0.12	−0.18	−0.25	−1.42
		4.0	0.15	0.01	−0.04	−0.09	−0.15	−0.20	−1.14
		5.0	0.20	0.01	−0.03	−0.08	−0.12	−0.18	−0.98

Table 7. Retrieval error, ΔC_{chl}, originating from the fluorescence of dissolved organic and phytoplankton ($\eta_{doc}(\lambda)$ is as given in the input data section), $C_{chl}^{input} = 2\mu\mathrm{g\,l^{-1}}$.

			Cdoc ($\mathrm{mgC\,l^{-1}}$)				
	η_{chl} (%)	C_{sm} ($\mathrm{mg\,l^{-1}}$)	0.5	1.0	2.0	5.0	10.0
ΔC_{doc}	0.7	0.5	0.17	0.37	0.65	0.95	0.97
		1.0	0.12	0.25	0.48	0.95	0.97
		2.0	0.08	0.17	0.34	0.86	0.80
		3.0	0.07	0.14	0.28	0.76	0.87
		4.0	0.06	0.12	0.25	0.69	0.95
		5.0	0.05	0.11	0.23	0.64	0.78
	3.0	0.5	0.35	0.66	0.99	0.97	0.90
		1.0	0.25	0.43	0.73	0.97	0.84
		2.0	0.18	0.29	0.49	0.91	0.89
		3.0	0.15	0.23	0.40	0.92	0.99
		4.0	0.13	0.20	0.35	0.82	0.93
		5.0	0.12	0.18	0.31	0.75	0.89

and negative, not exceeding, however, ~25% (table 8). If both C_{doc} and C_{chl} increase to $10\,\mathrm{mgC\,l^{-1}}$, and $15\,\mu\mathrm{g\,l^{-1}}$ respectively, ΔC_{sm} progressively decreases: the highest overestimation of C_{sm} occurs at lowest C_{doc} (table 8).

Within the explored ranges of the OAC concentrations and with $\eta_{chl} = 0.7\%$, C_{sm} is likely to be slightly overestimated (by ~1.5%) at low values of both C_{doc} and C_{chl} and more substantially overestimated (by ~25%) at high values of C_{chl} and low values of C_{doc} (table 8). C_{doc} is expected to be underestimated up to ~25% at low values of both C_{chl} and C_{sm}, and even up to ~50% at $C_{chl} = C_{sm} = 0$ (table 6). C_{chl} will be underestimated at any combinations of C_{doc} and C_{sm}: the underestimation can reach nearly 100% at high values of C_{doc} and low values of C_{sm} (table 7).

The OAC retrieval errors become accentuated if higher η_{chl} values are adopted. This is particularly so for dissolved organics and suspended minerals: at high concentrations of chlorophyll and low content of suspended minerals, C_{doc} may be

Table 8. Retrieval error, ΔC_{sm}, originating from the fluorescence of dissolved organic and phytoplankton fluorescence ($\eta_{doc}(\lambda)$ is as given in the input data section), $C_{sm}^{input} = 3\,\mathrm{mg\,l^{-1}}$.

			Cchl ($\mu\mathrm{g\,l^{-1}}$)						
	η_{chl} (%)	C_{doc} (mg/l)	0.5	1.0	2.0	3.0	4.0	5.0	15.0
ΔC_{sm}	0.7	0.5	−0.01	−0.02	−0.03	−0.04	−0.05	−0.07	−0.23
		1.0	−0.02	−0.02	−0.03	−0.04	−0.05	−0.07	−0.22
		2.0	−0.11	−0.01	−0.02	−0.03	−0.04	−0.06	−0.21
		5.0	−0.21	−0.15	−0.11	−0.03	0.02	0.00	−0.12
		10.0	−0.23	−0.25	0.00	−0.01	0.03	0.04	0.02
	3.0	0.5	−0.03	−0.06	−0.11	−0.17	−0.23	−0.30	−1.57
		1.0	−0.03	−0.06	−0.11	−0.17	−0.23	−0.30	−1.54
		2.0	−0.12	−0.05	−0.10	−0.16	−0.22	−0.29	−1.46
		5.0	−0.08	−0.13	−0.23	−0.16	−0.15	−0.21	−1.18
		10.0	−0.06	−0.05	−0.12	−0.16	−0.19	−0.41	−0.77

overestimated by a factor of ~5 (table 6), whereas at high C_{chl} and low C_{doc}, the content of suspended minerals may be overestimated by a factor of ~1.5 (table 8). Although the error of chlorophyll retrieval seems to be less sensitive to the value of η_{chl}, it nevertheless increases with increasing η_{chl}, the underestimation of C_{chl} being especially strong at high C_{doc} (table 7).

Our numerical experiments indicate that adequate OAC concentration retrievals are only possible if the fluorescence yields of chlorophyll and dissolved organics are known with reasonable confidence, i.e. experiments are needed for very different compositions of oceanic and inland waters.

6. Discussion and concluding remarks

The impact of transspectral processes on water leaving radiance $L_u(-0, \lambda)$ and, as a consequence, on the OAC vector retrieval is controlled by both in-water optical conditions and the illumination conditions at the water surface. Unlike the effect of water Raman scattering which can be only of limited importance in clear water nearly devoid of phytoplankton, dissolved organics and suspended minerals, the fluorescence of chlorophyll and dissolved organics is capable of influencing $L_u(-0, \lambda)$ and eventually the OAC concentration vector retrievals in both clear and turbid/absorbing waters.

This implies, in particular, that the colour of *natural* waters is not a sole consequence of absorption and scattering of light interaction in the water body, but is also due to fluorescence. The fluorescent emissions in water by phytoplankton chlorophyll and dissolved organics are potentially able to seriously modify the general regularities of water colour formation as compared to a purely absorbing and scattering liquid. Within the range of OAC concentrations explored in our simulations that frequently occur in oligotrophic and mesotrophic waters, the dominant wavelength, λ_{dom}, increasing with increasing concentrations of OAC, is not expected to tend to one and the same value (~570 nm) as it was predicted for water devoid of fluorophores, but to some *lower* values dependent on the actual combination of OAC concentrations.

Contributing to the radiance signal captured by a remote sensor, fluorescent emissions in water are inevitably bound to affect the retrieval results if they are

calculated with algorithms/procedures derived without due reference to transspectral effects. The degradation of the retrieval accuracy due to fluorescence by chlorophyll and dissolved organics is a function of the OAC concentration vector.

Our previous studies (Bukata *et al.* 1995, Pozdnyakov and Lyaskovsky 1999) demonstrated that in the case of waters rich in either one or several OAC, only water quality retrieval procedures like multivariate optimization techniques or neural networks are capable to cope with the inverse solution problems inherent in the optical complexity of such waters. Practical application of these sophisticated approaches requires the availability of a hydrooptical model (i.e. spectral values of OAC absorption and scattering cross sections) appropriate for the targeted water body.

In the light of our transspectral simulations, it seems justified to complement the required hydro-optical model with tabulated spectral values of the fluorescence yields η_{chl} and η_{doc}. Generally, both absorption and scattering cross sections as well as fluorescence yields are variable and water body- and season-specific.

Consequently, a further improvement of water quality retrieval accuracy needs the hydro-optical models specified above for major vegetation seasons and water areas/water bodies.

However, it is not unreasonable to expect (see e.g. Pozdnyakov *et al.* 1999) that the variety of such area- and season-specific models can be reduced to some typical ones (in terms of latitudinal zone, vegetation season, landscape type, anthropogenic loading), which can be applied either *per se* or in mutual combinations in different water bodies.

Given an appropriate hydro-optical model, the water quality retrieval can be realized as an iterative procedure. In a first step, the concentration vector is determined assuming that chlorophyll and dissolved organics did not fluoresce. From these tentatively retrieved concentrations, the contributions from fluorescence by chlorophyll and dissolved organics, R^f_{doc} and R^f_{chl}, are assessed in a second step. In a third step, the signal thus corrected for the effect of fluorescence is again processed to obtain a more realistic concentration vector.

Notwithstanding a certain degrading of operational efficiency of this retrieval procedure, it is noteworthy that with the modern computational facilities, it does not appear *excessively* time-consuming, since the R^f_{doc} and R^f_{chl}, models used in this scheme are sufficiently simple.

It is obvious, however, that the use of the suggested iterative procedure seems only reasonable if the error of the atmospheric correction is substantially lower than the one induced by the transspectral effects. This is presently not yet routinely attainable when dealing with coastal zone and inland waters, i.e. for cases when the fluorescence effects might be substantial.

References

Anonymous, 1957, *International Lighting Vocabulary* (Paris: Publication du Comité International d'Eclairage), **1**, 136.

Austin, R. W., 1974, The remote sensing of spectral radiance from below the ocean surface. In *Optical aspects of oceanography*, edited by N. G. Jerlov and E. Steeman Nielsen (London: Elsevier Publications), pp. 317–344.

Babin, M., Morel, A., and Gentili, B., 1996, Remote sensing of sea surface Sun-induced chlorophyll fluorescence: consequences of natural variations in the optical characteristics of phytoplankton and the quantum yield of chlorophyll *a* fluorescence. *International Journal of Remote Sensing*, **12**, 2417–2448.

BAKER, K. S., and SMITH, R. C., 1997, Irradiance transmittance through the air–water interface. In *Ocean Optics XII, Proceedings of the SPIE International Society of Optical Engineering*, **1302**, 556–565.

BARTLETT, J. S., 1996, *The influence of Raman scattering by seawater and fluorescence by phytoplankton on ocean colour*. MSc Thesis (Halifax: Dalhousie University).

BARTLETT, J. S., 1997, A comparison of models of sea-surface reflectance incorporating Raman scattering by water. In *Ocean Optics XII, Proceedings of the SPIE International Society of Optical Engineering*, **2963**, 592–602.

BARTLETT, J. S., VOSS, K. J., SATHYENDRANATH, S., and VODACEK, A., 1998, Raman scattering by pure water and seawater. *Applied Optics*, **37**, 3324–3332.

BERWALD, J., STRAMSKI, D., MOBLEY, C. D., and KIEFER, D. D., 1998, Effect of Raman scattering on the average cosine and diffuse attenuation coefficient of irradiance in the ocean. *Limnolology and Oceanography*, **43**, 564–576.

BUKATA, R. P. JEROME, J. H., KONDRATYEV, K. YA., and POZDNYAKOV, D. V., 1991, Estimation of organic and inorganic matter in inland waters: Optical cross sections of Lakes Ontario and Ladoga, *Journal of Great Lakes Research*, **17**, 461–469.

BUKATA, R. P. JEROME, J. H., KONDRATYEV, K. YA., and POZDNYAKOV, D. V., 1995, *Optical properties and Remote Sensing of Inland and Coastal Waters* (Boka Raton: CRC Press).

BUKATA, R. P., JEROME, J. H., KONDRATYEV, K. YA., and POZDNYAKOV, D. V., 1997, Modelling the radiometric color of inland waters: Implications to a) remote sensing and b) limnological color scales. *Journal of Great Lakes Research*, **23**, 254–269.

BUKATA, R. P., POZDNYAKOV, D. V., JEROME, J. H., and TANIS, F. J., 1999, Validation of a radiometric color model applicable to optically-complex water bodies. *Remote Sensing of Environment* (submitted).

BURT, W. V., 1953, A note on the reflection of diffuse radiation by the sea surface. *Transactions of the American Geophysical Union*, **34**, 199–200.

COBLE, P. G., and BROPHY, M. M., 1996, Investigation of the geochemistry of dissolved organic matter in coastal waters using optical properties. In *Ocean Optics XII, Proceedings of the SPIE International Society of Optical Engineering*, **494**, 56–61.

CULVER, M. E., and PERRY, M. J., 1997, Calculation of solar-induced fluorescence in the surface and subsurface waters. *Journal of Geophysical Research*, **102**, 10 563–10 572.

FISCHER, J., and KRONFELD, U., 1990, Sun-stimulated chlorophyll fluorescence. 1: Influence of oceanic properties. *International Journal of Remote Sensing*, **11**, 2125–2147.

GORDON, J. I., 1969, *Directional radiance (luminance) of the sea surface*. (La Jolla: Scripps Institution of Oceanography), CA 92093, SIO Ref. 69-20.

GORDON, H. R., 1979, Diffuse reflectance of the ocean: the theory of its augmentation by chlorophyll a fluorescence at 685 nm. *Applied Optics*, **18**, 1161–1166.

GORDON, H. R., 1989, Dependence of the diffuse reflectance of natural waters on the sun angle. *Limnology and Oceanography*, **34**, 1484–1489.

GORDON, H. R., BROWN, O. B., and JACOBS, M. M., 1975, Computed relationships between the inherent and apparent optical properties of a flat homogeneous ocean. *Applied Optics*, **14**, 417–427.

GREEN, S., and BLOUGH, N. V., 1994, Optical absorption and fluorescence properties of chromophoric dissolved organic matter in natural waters. *Limnology and Oceanography*, **39**, 1903–1916.

GREGG, W. W. and CARDER, K. L., 1990, A simple spectral solar irradiance model for cloudless maritime atmospheres. *Limnology and Oceanography*, **35**, 1657–1675.

HALTRIN, V. I., and KATTAWAR, G. W., 1991, *Effects of Raman Scattering and Fluorescence on Apparent Optical Properties of Sea Water* (Texas: Texas A&M University).

HALTRIN, V. I., and KATTAWAR, G. W., 1993, Self-consistent solutions to the equation of transfer with elastic and inelastic scattering in ocean optics: 1. Model. *Applied Optics*, **32**, 5356–5367.

JERLOV, N. G., 1976, *Marine Optics* (Amsterdam: Elsevier), Oceanography Series, **14**.

JEROME, J. H., BUKATA, R. P., and BRUTON, J. E., 1988, Utilising the components of vector irradiance to estimate the scalar irradiance in natural waters. *Applied Optics*, **27**, 4012–4018.

KIRK, J. T. O., 1976, Yellow substance (Gelbstoff) and its contribution to the attenuation of photosynthetically active radiation in some inland and coastal south-eastern Australian waters. *Australian Journal of Marine Freshwater Research*, **27**, 61–71.

KIRK, J. T. O., 1981, Monte Carlo study of the nature of the underwater field in, and the relationships between optical properties of, turbid yellow water. *Australian Journal of Marine Freshwater Research*, **32**, 517–532.

KIRK, J. T. O., 1984, Dependence of relationship between inherent and apparent optical properties of water on solar altitude. *Limnology and Oceanography*, **29**, 350–356.

KONDRATYEV, K. YA., and POZDNYAKOV, D. V., 1996, Ozone depletion-induced UVB radiation impact on aquatic ecosystems. II. Hydrooptical aspects of the problem. *Earth Observation and Remote Sensing*, **6**, 105–114.

KONDRATYEV, K. YA., POZDNYAKOV, D. V., and ISAKOV, V. YU., 1990, *Hydrooptical Radiation Experiments on Lakes* (Leningrad: Nauka Publishing Co.).

KONDRATYEV, K. YA., POZDNYAKOV, D. V., and PETTERSSON, L. H., 1998, Water quality remote sensing in the visible. *International Journal of Remote Sensing*, **19**, 957–979.

KONDRATYEV, K. YA., FILATOV, N. N., and POZDNYAKOV, D. V., 1999, *Limnology and Remote Sensing: A Contemporary approach* (Chichester: Springer-Praxis).

LEE, Z. P., CARDER, K. L., HAWES, S. K., STEWARD, R. G., PEACOCK, T. G., and DAVIS, C. O., 1994, Model for the interpretation of hyperspectral remote-sensing reflectance. *Applied Optics*, **33**, 5721–5732.

MARSHALL, B. R., and SMITH, R. C., 1990, Raman scattering and in-water ocean optical properties. *Applied Optics*, **29**, 71–84.

MOREL, A., 1980, Optical properties of pure water and sea water. In *Optical Aspects of Oceanography*, edited by N. G. Jerlov and N. Steeman (London: Academic Press), pp. 1–24.

PETROVA, N. A., 1990, *Phytoplankton successions driven by anthropogenic eutrophication in large lakes* (Leningrad: Nauka Publishing Co.).

POZDNYAKOV, D. V., and LYASKOVSKY, A. V., 1999, A model study of the adequacy of some case II water quality retrieval algorithms suggested for inland and marine coastal waters. *Earth Observation and Remote Sensing*, **1**, 70–78.

POZDNYAKOV, D. V., LYASKOVSKY, A. V., TANIS, F. J., and LYZENGA, D. R., 1999, Modeling of apparent hydrooptical properties and retrievals of water quality in the Great Lakes for SeaWiFS: a comparison with in situ measurements. *Proceedings of the IGARRS'99 Conference, Hamburg, Germany, 27 June–1 July, 1999, vol. II*, pp. 1143–1147.

POZDNYAKOV, D. V., SHUCHMAN, R. A., LYASKOVSKY, A. V., TANIS, F. J., and LYZENGA, D. R., 2000, Experimental evidence of dissolved organics fluorescence impact on upwelling radiance in Saginaw Bay of Lake Huron. *Proceedings of the ERIM Conference on Marine and Coastal Environments, Charleston, Ill. USA, May 1–3, 2000, vol. I*, pp. 31–38.

PREISENDORFER, R. W., 1957, Exact reflectance under a cardioidal luminance distribution. *Quarterly Journal of the Royal Meteorological Society*, **83**, 540–551.

SATHYENDRANATH, S., and PLATT, T., 1998, Ocean-color model incorporating transspectral processes. *Applied Optics*, **37**, 2216–2227.

SIEGEL, H., GERTH, M., and BECKERT, M., 1997, Variation of specific optical properties and their influence on measaured and modelled spectral reflectances in the Baltic Sea. In *Ocean Optics XII, Proceedings of the SPIE International Society of Optical Engineering*, **2963**, 526–531.

SMITH, R. C., and BAKER, K. S., 1981, Optical properties of the clearest natural waters (200–800 nm). *Applied Optics*, **20**, 177–184.

SUGIHARA, S., KISHINO, M., and OKAMI, N., 1984, Contribution of Raman scattering to upward irradiance in the sea. *Journal of Oceanographic Society of Japan*, **40**, 397–404.

VODACEK, A., GREEN, S. A., and BLOUGH, N. V., 1994, An experimental model of the solar-stimulated fluorescence of chromophoric dissolved organic matter. *Limnology and Oceanography*, **39**, 1–11.

VOHEN, H., 1997, Laboratory measurement of angular distribution of light scattered by phytoplankton and silt. *Limnology and Oceanography*, **42**, 307–318.

WATERS, K. J., 1995, Effects of Raman scattering on water-leaving radiance, *Journal of Geophysical Research*, **100**, 13 151–13 161.